CHEMICAL ENGINEERING TRANSACTIONS
VOL. 86, 2021
A publication of AIDIC
The Italian Association of Chemical Engineering
Online at www.cetjournal.it
Guest Editors: Sauro Pierucci, Jiří Jaromír Klemeš

ISBN 978-88-95608-84-6; **ISSN** 2283-9216

Assessment of LNG Fire Scenarios on Board of LNG-Fuelled Ships

Tommaso Iannaccone[a], Giordano E. Scarponi[a], Byongug Jeong[b], Valerio Cozzani[a,*]

[a]LISES - Dipartimento di Ingegneria Civile, Chimica, Ambientale e dei Materiali, Alma Mater Studiorum - Università di Bologna, via Terracini, 28, 40131 Bologna, Italy.
[b]Department of Naval Architecture, Ocean and Marine Engineering, University of Strathclyde, 100 Montrose Street, G4 0LZ, Glasgow, UK
valerio.cozzani@unibo.it

Decarbonization represent one of the main challenges of the maritime transport sector for the near future. As recent international environmental regulations have set more stringent emission limits, the use of liquefied natural gas (LNG) as alternative ship fuel has proven to be a viable and less-polluting solution, compared to conventional oil-based fuels. However, LNG is a highly flammable substance and safety aspects need to be assessed thoroughly, especially for its use on board passenger ships.
Two different gas engine concepts are typically used for ship propulsion: Low-Pressure Dual Fuel (LPDF) and High-Pressure Dual Fuel (HPDF) engines. Regardless of the gas engine technology, the fuel gas supply system process equipment is located inside a specific enclosed space, the fuel preparation room (FPR), that can be sited below deck. Given this background, this study aims to investigate the consequences of LNG pool fires occurring inside a confined space, assessing the influence of different operating conditions. Credible loss of containment events were identified to define the characteristics of LNG pools. Furthermore, LNG pool fires were simulated using the fire dynamic simulator (FDS) to estimate the radiation heat flux received by the process equipment installed inside the FPR and to assess the possibility of experiencing accident escalation on board. To evaluate the effect of forced mechanical ventilation of the FPR, two different cases were modelled: one assuming the standard functioning of the ventilation system, while the other one considered a halted air supply inside the FPR with a working exhaust system only. The outcomes of this study provide useful data for the consequence estimation of small-scale LNG pool fires occurring inside enclosed spaces, also addressing the possibility of accident escalation on board LNG-fuelled ships.

1. Introduction

The design, construction and operation of ships using gaseous fuels is covered by the International Maritime Organization's IGF Code (IMO, 2015). According to the IGF Code, FPRs can be designed either as "gas safe", or as "ESD-protected" spaces. In the former case any failure within the fuel system cannot lead to a release of fuel gas, whereas for ESD-protected FPR, a single failure may result in a gas release into the space and subsequent activation of the ESD system. Furthermore, the IGF code requires that the fuel must be supplied from the FPR to the engine room through double wall pipes. For such reason, the present study was only focused on accidents occurring inside an ESD-protected FPR, for which double-walled pipes are not mandatory and, consequently, release events cannot be excluded.
Several works addressed the modelling of enclosure fires: theoretical basis of this phenomena can be found in the works by (Quintiere, 2006), whereas a general summary of experimental fire tests in confined and ventilated multi-compartments is presented by Audouin et al., (2013). A number of numerical and experimental studies, focused on the consequence modelling of large LNG spills occurring in an open environment, either on land or water, while other estimated the consequence of smaller LNG pool fires (Pio et al., 2019), including their impact

on storage tanks (Iannaccone et al., 2020). However, the reviewed literature lacks a study aimed at evaluating the consequences of small-scale LNG pool fires occurring inside confined spaces. The present work can be viewed as a first attempt to fill this research gap, providing a preliminary consequence estimation of enclosure LNG pool fires occurring in a ventilated compartment.

2. Modelling approach

The present study focused on the evaluation of LNG pool fire consequences inside the FPR of a typical roll on/roll off ferry ship, which is currently the most common type of LNG-fuelled vessel, according to DNV-GL, (2020). Moreover, this kind of ships can either be fuelled using Low-Pressure (LP) or High-Pressure (HP) systems, allowing for a comparison between these types of Fuel Gas Supply Systems (FGSS) from a safety perspective. A description of the mentioned LNG FGSS can be found in the work by Iannaccone et al., (2020) along with block diagrams. Preliminary to the CFD modelling, the process units, and the operative conditions of each FGS system were identified, providing the basis for the Loss of Containment events (LOC) categorization, which was carried out considering two possible situations for liquid releases. Following the guidance by Uijt de Haag and Ale (2005) LOC types R4 (Pipe leak, continuous release from a hole having 10% of pipe diameter) and R5 (continuous release from the full-bore pipe) were considered for the HP Fuel gas pump of the HPDF system and for the inlet connection of the LNG Vaporizer featured in the LP FGSS. Release events were assumed to remain undetected for at least 90 s, as this was assumed as the required timeframe for ESD system intervention. A summary of the considered LOC events, along with process conditions and estimated release rates and spilt mass is reported in Table 1.

Table 1: Summary of the main characteristics of assessed LOC events

Process unit	Vol. Flowrate [m^3/s]	Pressure [bar]	Temperature [K]	LOC Type	Release rate [kg/s]	Spilt mass [kg]
HP FGSS						
HP Fuel gas pump	7.19	300	146	R4	1.215*	109.35
				R5	1.215*	109.35
LP FGSS						
LNG Vaporizer	7.49	7	133	R4	1.018	91.62
				R5	1.215*	109.35

* Assumed as 150% of ordinary mass flowrate

In absence of more detailed specifications, release rates were limited to up 150% of the ordinary mass flowrate to approximatively account for the loss of pressure head in the line and the consequent shift of the pump operating point as suggested by Uijt de Haag and Ale (2005).

The dimensions of the pools resulting from the considered releases were estimated using the pool evaporation model developed by Briscoe and Shaw (1980) that also allows to evaluate the mass evaporating from the pool, which was used as input for the FDS simulations. The geometry of the FPR was reproduced in FDS to model the effects of two different pool fire scenarios: one larger pool resulting from the HP pump release, and a slightly smaller pool formed ensuing the R4 LOC event affecting the vaporiser inlet. Furthermore, the influence of two different operative conditions of the FPR mechanical ventilation system was assessed.

2.1 Case study definition

The FPR of the reference case ship is 23 m long, 5.1 m high and 5.5 m wide. Side walls of the FPR were assumed to be lined with class A-60 material, following the requirements set by the IGF code (IMO, 2015). Among the minimum safety systems required by the IGF code for ESD-protected spaces, all confined spaces must be fitted with mechanical ventilation systems providing at least 30 air changes per hour.

To reproduce generic conditions inside the FPR, five square exhaust vents with a surface of 1 m^2 each were assumed to be located on the longitudinal midsection of the FPR ceiling, equally distanced. Similarly, two square 1 m^2 ventilation supply vents were placed at the transversal midsection of the FPR, at 1 m height. The overall supply and exhaust capacity of the ventilation system reproduces the required 30 air changes per hour that are equal to a volumetric flowrate of 18,800 m^3/h. A schematic overview of the computational domain is shown in Figure 1, while the exact location of FPR features and pool fire are specified in Table 2.

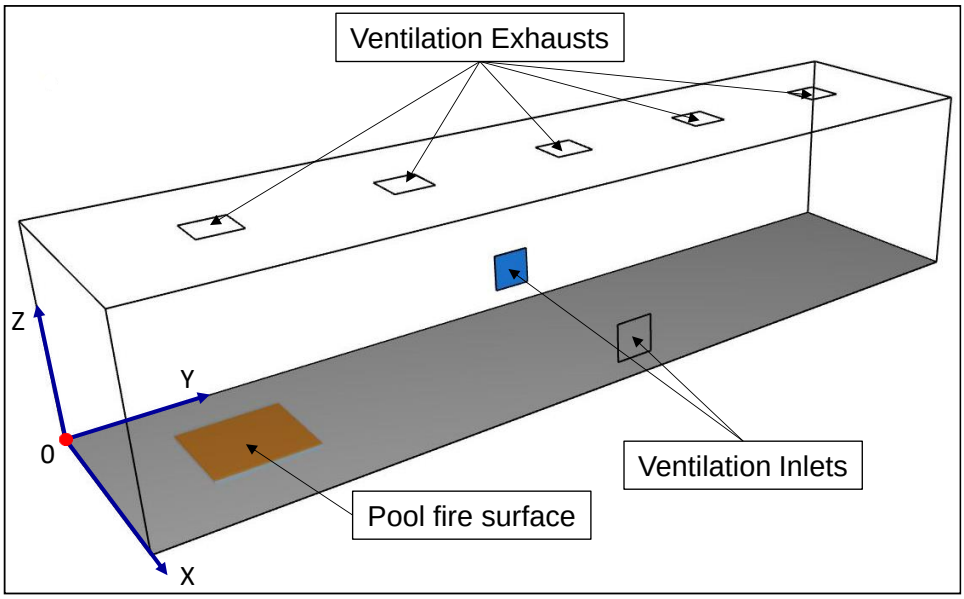

Figure 1: Schematic view of the FPR modelled in FDS. The pool fire surface, even if displayed as a square, is modelled by defining a circular vent.

Table 2: Coordinates of pool fire centre and mechanical ventilation vents for the modelled FPR. Refer to Figure 1 for additional reference.

Item	Domain coordinates [m]		
	x-axis	y-axis	z-axis
Pool Centre	2.725	3.000	0.000
Exhaust vent #1	2.725	2.875	5.100
Exhaust vent #2	2.725	7.188	5.100
Exhaust vent #3	2.725	11.500	5.100
Exhaust vent #4	2.725	15.813	5.100
Exhaust vent #5	2.725	20.125	5.100
Supply vent #1	0.000	11.500	1.000
Supply vent #2	5.500	11.500	1.000

2.2 Numerical setup

To capture the influence of the ventilation system on pool fire development, two different operating modes were considered: one assumed a normal-operating ventilation system (i.e., with both fresh air supply and exhaust), while the other reproduced a halted air supply with operating exhaust vents. These operating modes were combined with different pool diameters, estimated with the Briscoe and Shaw model: a larger pool, resulting from LOCs R4/R5 affecting the HP Fuel gas pump of the HPDF, and a smaller one, having a diameter of 2.12 m, estimated for a R4 LOC type affecting the inlet of the LP FGSS LNG Vaporizer. Such combination led to the definition of four different simulation cases, summarized in Table 3.

Table 3: Main characteristics of the FDS simulation cases.

Case ID	Pool diameter [m]	Ventilation	Cell number
HP - 1	2.36	No (exhaust only)	322,575
HP - 2		Yes (in/out)	
LP - 1	2.12	No (exhaust only)	
LP - 2		Yes (in/out)	

As reported by McGrattan et al., (2015b), uniform meshing is preferred since FDS is a CFD tool based on the large eddy simulation turbulence model, thus the computational domain was subdivided into cells having a uniform size of 0.15 m. Such cell dimension was chosen following the recommendations given by the U.S. Nuclear Regulatory Commission (2016) in their report on the verification and validation of selected fire models.

All simulations were run considering a maximum duration of 90 s and a variable time step, initially set at 0.01 s and limited by a stability constraint on the Courant-Friedrichs-Lewy number (see McGrattan et al. (2015b) for additional details). Initial temperature and pressure inside the FPR were set at 15 °C and 1 atm respectively, considering normal operating onboard conditions. To avoid introducing uncertainties related to LNG composition, this was assumed as pure methane. A detailed analysis of the effects of different LNG compositions over thermal characteristics of small-scale pool fires can be found in the work by Cozzani et al., (2019). Since the determination of a pool spread rate could be influenced by numerous factors for the specific cases under analysis, such as the ship movements, a simplified approach was followed to reproduce the spreading of the LNG pools in the simulations. The pool fires were defined using a circular vent surface having the same area as the maximum pool area estimated by Briscoe and Shaw model (1980). To model the time variation of the pool evaporation rates, a prescribed boundary condition was given on the pool fire surface, specifying a time ramp of evaporated mass flux values estimated using the previously mentioned pool evaporation model. Following a rapid increase of the evaporation flux during the first seconds of the simulation, the values stabilize around 0.246 and 0.257 kg/m^2 s for HP and LP pools, respectively.

Methane combustion reaction was modelled using a two-step Simple Chemistry kinetic model as suggested by Lock et al. (2008). The two-step scheme basically converts all the carbon in the fuel molecule to CO and Soot in the first step, and then oxidizes most of the CO and Soot to form CO_2 in the second step. The fuel hydrogen atoms can either form H_2 or H_2O in the first step as well.

$$C_xH_y + \nu_{O_2,1} O_2 \rightarrow \nu_{H_2O,1} H_2O + \nu_{CO,1} CO + \nu_{S,1} Soot \quad (1)$$

$$\nu_{H_2O,1} H_2O + \nu_{CO,1} CO + \nu_{S,1} Soot + \nu_{O_2,2} O_2 \rightarrow \nu_{H_2O,1} H_2O + \nu_{CO_2} CO_2 + \nu_{CO,2} CO + \nu_{S,2} Soot \quad (2)$$

The post-flame yields of CO, H_2 and Soot were all set equal to the default value of zero for the present analysis, in the absence of more detailed data. However, it should be remarked that the two-step model acknowledges the fact that CO and Soot are present at much higher concentrations within the flame envelope than their post-flame yields would suggest (McGrattan et al., 2019).
To consider the fire suppression due to oxygen depletion inside the FPR, the FDS Flame Extinction model was enabled. Between the two options available, the simpler “Extinction 1” model was chosen, which prevents the solver to model combustion inside cells with an oxygen concentration below a lower limiting value. Further details on the Flame Extinction model can be found in the FDS Technical Reference Guide (McGrattan et al., 2015).

3. Results and discussion

The independence of simulation results from the chosen calculation grid was assessed comparing the predicted Heat Release Rate (HRR) values for grids with different cell sizes. Satisfactory results were obtained considering grids with element sizes of 0.10 and 0.20 m: HRR differences with respect to the used calculation grid were comprised between 1% and 4%.
The effects induced by the different ventilation conditions can be observed in Figure 2. Focusing on the oxygen concentration, it can be observed that generally this value decreases with time, as oxygen is consumed by the combustion reaction. This decreasing trend is similar for both cases LP–1 (Exhaust only) and HP–2 (Ventilation On) for the first 30 s of combustion, then the oxygen rate of consumption decreases until reaching an apparent steady state for case LP–2, while without fresh air inlet the concentration continues to drop until reaching values close to zero around 70 s from the fire ignition. This is an evident consequence of the combined effect of fire consumption and air extraction from the compartment and a key factor governing the evolution of the pool fire inside the FPR.
The decreasing trend showed by the HRR curve of case LP–1 reported in Figure 2 confirms that the oxygen concentration plays a determinant role in the evolution of an enclosure fire. For this case, the pool fire starts to grow weaker when O_2 concentration drops below 6% vol. (around 35 s from fire ignition). As evident from the comparison with case HP-2, the oxygen depletion is the cause of fire self-extinction, which does not occur in presence of air inlets, even if a sensible reduction of the HRR, about 45% lower than the modelled peak value of 65,000 kW, can be observed during the simulation for this latter case. Analogous results were obtained for cases LP-2 ad HP-1, which are not reported in Figure 2 for sake of clarity.

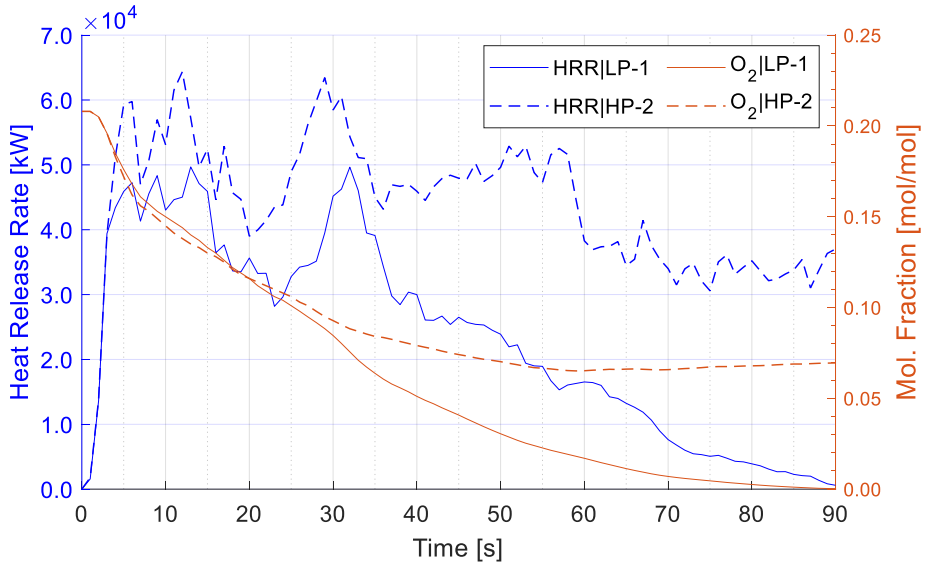

Figure 2: Comparison of the HRR (left y-axis) and O_2 concentration (right y-axis) for cases LP-1 and HP-2.

Contour plots of the time-averaged incident heat flux measured on the opposite wall from pool fire location are shown in Figure 3. The incident radiation fluxes received by FPR boundaries are significant higher for the cases HP-2 and LP-2, when air inlets are working, and the pool fire lasts for the whole duration of the simulation. Values ranging between 140 and 30 kW/m^2 are reached. For all the cases the wall region subject to the highest flux is located in the upper half of the wall, closer to the FPR ceiling. Lower heat flux values are predicted close to the floor, with values below 50 kW/m^2 for heights less than 1 m for cases HP-1 and LP-1. Observing panels c and d, a zone subject to a slightly higher radiation flux can be noticed at the ground level, approximately at the mid-section of the FPR. The presence of this region, not predicted for cases HP-1 and LP-1, might be explained considering the pool fire duration, which lasts for the entire simulation when considering fresh air inlet, thus contributing to increase the time-averaged heat fluxes around ground level.

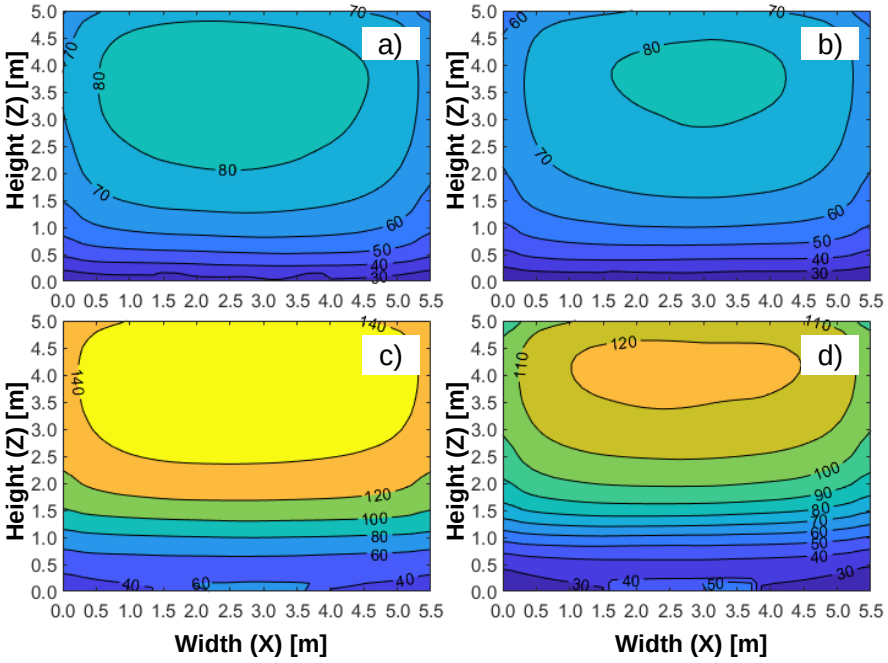

Figure 3: Comparison of time-averaged contours of incident radiation heat flux (in kW/m^2) for the XZ plane at Y=23 m (opposite wall from pool fire location). Panel a) shows case HP-1; b) case LP-1; c) case HP-2; d) case LP-2.

4. Conclusions

The effects of accidental LNG pool fires occurring inside an ESD-protected FPR were investigated considering a ship case study suitable for both high- and low-pressure dual fuel systems. Pool fires with two different diameters were considered, resulting from releases affecting the high-pressure fuel pumps and the LNG vaporiser featured in the LPDF system. Findings of the CFD modelling showed little differences between consequences stemming from HPDF and LPDF systems, as LNG pools having similar dimensions will be formed. Conversely, substantial differences in the dynamic evolution of the enclosure pool fire were observed when comparing the results obtained assuming different operating modes of the FPR mechanical ventilation system. A strong reduction of the pool fire HRR was observed around 35 seconds after fire ignition, with a simultaneous depletion of the oxygen concentration inside the FPR that eventually lead to the self-extinction of the pool fire when no fresh air inlet was considered, as opposite to the situation assuming air to be drawn in the enclosure by the ventilation system. In this latter case the oxygen concentration reaches an equilibrium value sufficient to maintain the combustion process for the entire duration of the simulation. Regardless of the operative profile of the ventilation system, the modelled pool fires can generate incident heat fluxes high enough to undermine the structural integrity of exposed surfaces of the FPR and of the process equipment installed therein, possibly leading to accident escalation.

From this it can be concluded that in case of a late activation of the ESD system, LNG pool fires occurring inside the FPR might give rise to dangerous situations for the safety of both passengers and ship structures due to consequence severity. The results of this study can provide a starting point for future parametric risk assessment studies aimed at evaluating the influence of structural design choices and operational profiles on the safety level of LNG-fuelled ships' FPRs. Lastly, safety recommendations can be drawn from the outcomes of this analysis, further improving the existing regulatory provisions.

References

Audouin, L., Rigollet, L., Prétrel, H., Le Saux, W., Röwekamp, M., 2013, OECD PRISME project: Fires in confined and ventilated nuclear-type multi-compartments - Overview and main experimental results, Fire Safety Journal, 62, 80-101.

Briscoe, F., Shaw, P., 1980, Spread and evaporation of liquid, Progress in Energy and Combustion Science, 6, 127–140.

Cozzani, V., Pio, G., Salzano, E., 2019, Numerical Simulation of Multi-Component LNG Pool Fire, Chemical Engineering Transactions, 74, 1357–1362.

DNV-GL, 2020, Alternative Fuels Insight Platform <store.veracity.com/da10a663-a409-4764-be66-e7a55401275a> accessed 26.6.20.

Iannaccone, T., Scarponi, G.E., Landucci, G., Cozzani, V., 2020, LNG tanks exposed to distant pool fires: a CFD study, Chemical Engineering Transactions, 82, 373–378.

Iannaccone, T., Landucci, G., Tugnoli, A., Salzano, E., Cozzani, V., 2020, Sustainability of cruise ship fuel systems: Comparison among LNG and diesel technologies, Journal of Cleaner Production, 260, 121069.

International Maritime Organization (IMO), 2015, International code of safety for ships using gases or other low-flashpoint fuels (IGF CODE), London, UK.

Lock, A., Bundy, M., Johnsson, E.L., Hamins, A., Ko, G.H., Hwang, C., Fuss, P., Harris, R., 2008. Experimental study of the effects of fuel type , fuel distribution , and vent size on full-scale underventilated compartment fires in an ISO 9705 Room, NIST Technical Note 1603. Gaithersburg MD, USA.

McGrattan, K., Hostikka, S., McDermott, R., Floyd, J., Vanella, M., 2019. Fire Dynamics Simulator User's Guide, NIST Special Publication 1019. Gaithersburg, MD, USA

McGrattan, K., Hostikka, S., McDermott, R., Floyd, J., Weinschenk, C., Overholt, K., 2015, Fire Dynamics Simulator Technical Reference Guide Volume 1: Mathematical Model, NIST Special Publication 1018, Gaithersburg, MD, USA.

Pio, G., Carboni, M., Iannaccone, T., Cozzani, V., Salzano, E., 2019, Numerical simulation of small-scale pool fires of LNG, Journal of Loss Prevention in the Process Industries, 61, 82–88.

Quintiere, J.G., 2006, Fundamentals of Fire Phenomena, John Wiley & Sons Ltd, Chichester, UK.

Stroup, D., Lindeman, A., McGrattan, K., Peacock, R., Overholt, K., Joglar, F., LeStrange, S., Montanez, S., 2016, Verification and validation of selected fire models for nuclear power plant applications, Washington, D.C., USA.

Uijt de Haag, P.A.M., Ale, B.J.M., 2005, Guidelines for quantitative risk assessment (Purple Book), third. ed, Committee for the Prevention of Disasters, The hague, The Netherlands.